ELSEVIER

S1359-835X(96)00042-5

Composites Part A **27A** (1996) 833–838

S1359-835X/96/$15.00

A study of transcrystalline polypropylene/single-aramid-fibre pull-out behaviour using Raman spectroscopy

M. Heppenstall-Butler, D. J. Bannister and R. J. Young*
Manchester Materials Science Centre, UMIST/University of Manchester, Grosvenor Street, Manchester M1 7HS, UK

The pull-out behaviour of isotactic polypropylene/Twaron D1056 single-fibre composites was investigated. Three matrix morphology types, two transcrystalline [fast-cooled (FCTC) and slow-crystallized (SCTC)] and one spherulitic [slow-crystallized (SCS)], were compared. The detailed point-to-point stress distributions along the embedded fibres were measured during pull-out using Raman spectroscopy. These stress distributions were modelled using a partial debonding theory, and it was found that the debond shear stress (τ_{max}) was of the order of 10 MPa for the three morphologies. Analysis of the pull-out data revealed that the mean interfacial frictional shear stress (τ_i) of the FCTC and SCTC samples is similar at ~2.2 MPa, higher than that of the SCS samples (~1.5 MPa).

(Keywords: transcrystallinity; pull-out tests; composites; Raman spectroscopy)

INTRODUCTION

The interface in a composite is very important in controlling its properties[1]. Considerable work has been done to describe interfaces quantitatively in a wide range of composites. An interface widely studied is that between reinforcing fibres and thermoplastic matrices[2–6], where the phenomenon of transcrystallinity[5–8] is often found. Unfortunately, little is known about the effect of transcrystallinity on interfacial parameters although some research[4,9–13] suggests that the effect is small, or negligible.

The use of Raman spectroscopy to follow the stress distribution along aramid fibres during pull-out from epoxy resins is now well documented[14,15]. Previous work[16] introduced the use of Raman spectroscopy in mapping the effect of an inhomogeneous semicrystalline polymer matrix on the residual stress distribution in an embedded aramid fibre. This work compares the fibre stress distributions during pull-out from transcrystalline and non-transcrystalline matrices as measured using Raman spectroscopy. Analysis of these distributions has allowed the interfacial parameters to be determined.

* To whom correspondence should be addressed

EXPERIMENTAL

All the composites studied were composed of SY6100 isotactic polypropylene (iPP) (melt flow index 11, $M_w = 270\,000$) and D1056, high modulus (103 GPa), reduced standard finish Twaron aramid fibres. These were kindly supplied by Dr J. L. Thomason of Shell Research and are materials that were used in previous publications about transcrystallinity by Thomason and van Rooyen[5,6].

A Linkham THMS600 hot-stage was used for sample preparation with an argon atmosphere to prevent degradation of the matrix by the fibre[17]. Each sample was made by placing a single fibre between two small strips of iPP, melting the iPP between glass cover slips separated by spacers, compressing the whole to the thickness of the spacers, then cooling through one of three thermal histories. The three thermal histories will be referred to a FCTC (fast-cooled transcrystalline), SCTC (slow-crystallized transcrystalline) and SCS (slow-crystallized spherulitic). Samples were compressed during the first minute at 200°C, thus allowing 9 min blank melting before the thermal history was imposed:

- FCTC $+50\,K\,min^{-1}$ to 200°C, 200°C for 10 min, $-2.5\,K\,s^{-1}$ to 15°C;
- SCTC $+50\,K\,min^{-1}$ to 200°C, 200°C for 10 min, $-10\,K\,min^{-1}$ to 130°C, 130°C for 70 min, $-10\,K\,min^{-1}$ to 15°C;

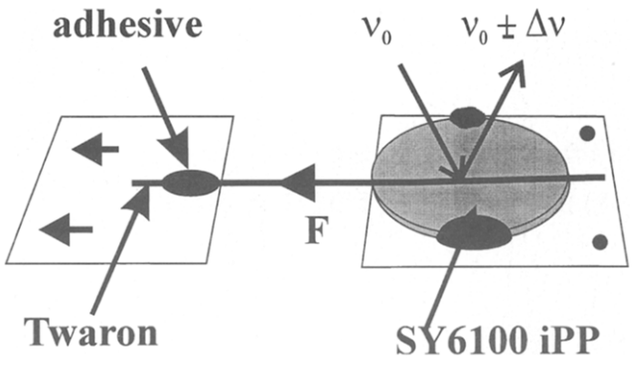

Figure 1 Diagram showing a pull-out sample with a schematic representation of the Raman effect

a SPEX 1000 M single monochromator which selected wavenumbers containing the 1610 cm^{-1} band from the aramid fibre[19]. The Raman spectrum (10 s exposure) was collected using a Wright Instruments charge-coupled device (CCD) camera cooled with liquid nitrogen[14].

The residual stresses along the fibre were measured before pull-out. Raman spectra were obtained along the fibre at 10, 20 or 50 μm intervals from 200 μm outside the matrix to well inside the matrix. Thus, from the unstresses free fibre spectra, the wavenumber for zero applied stress was found for each sample. Having measured the residual stresses, the free fibre was pulled to exert a small fixed strain. Raman spectra were then

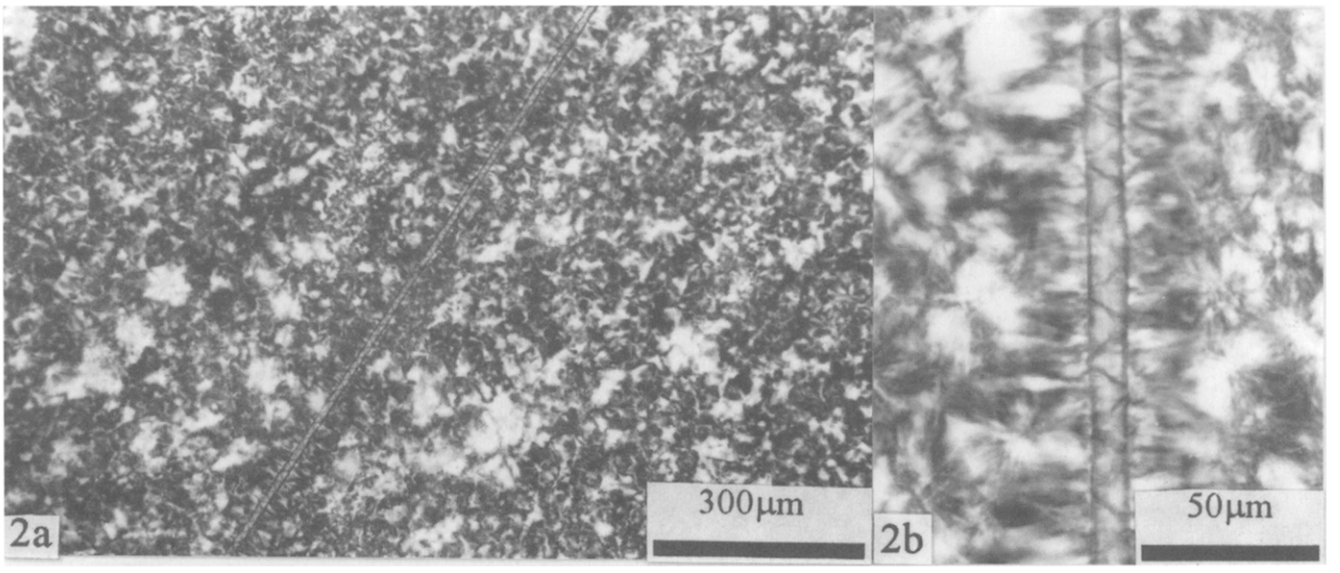

Figure 2 Optical micrographs of an FCTC sample showing (a) the fine transcrystalline layer and surrounding matrix spherulites, and (b) continuous kink bands along the fibre (crossed polarizers)

- SCS $+50\,K\,min^{-1}$ to 200°C, 200°C for 10 min, $-10\,K\,min^{-1}$ to 140°C, 140°C for 300 min, $-10\,K\,min^{-1}$ to 15°C.

This process resulted in flat oval samples with a thickness of $103 \pm 3\,\mu$m, and a width 2.5 to 5 mm. Thus 2.5 to 5 mm of fibre was embedded in each sample.

For pull-out tests, the samples were fixed to their lower glass cover slip using cyanoacrylic adhesive, then the whole was fixed to a glass slide so that the emergent fibre end protruded from the glass slide, as shown in *Figure 1*. The glass slide was then gripped in a miniature material tester (Rheometric's Ltd 'Minimat') and the free fibre was fixed to another glass slide gripped by the opposing crosshead. The free fibre length[18] was kept to below 2 mm.

With the free fibre slack, the Minimat was placed on the $X-Y$ stage of an Olympus BH-2 microscope, modified to focus the 632.8 nm red line of a 15 mW HeNe laser (polarized parallel to the fibre axis) to a $\sim 5\,\mu$m spot on the fibre inside the matrix using a $\times 50$ objective lens. The scattered radiation from the sample was then transmitted through a set of collection optics to obtained point-to-point from the fibre outside the matrix to deep inside until the stress remained unchanged. The stress was increased incrementally with the stress distribution measured by Raman spectroscopy after each increase[15].

The calibration used for the 1610 cm^{-1} Raman band was 4 cm^{-1}/GPa (refs 20–22).

RESULTS

Figures 2a, *3a* and *4a* show the morphologies produced by each thermal history. FCTC and SCTC samples possessed transcrystallinity, whereas SCS was wholly spherulitic. The average approximate spherulite size for FCTC samples was 20 μm, whereas that for SCTC and SCS samples was nearer 100 μm. The high magnification inserts, *Figures 2b*, *3b* and *4b*, show kink bands in the Twaron fibres. These were produced during cooling from the crystallization temperature for SCTC and SCS, or below 80°C during the cooling of the FCTC samples. The distribution of kink bands along the embedded fibre

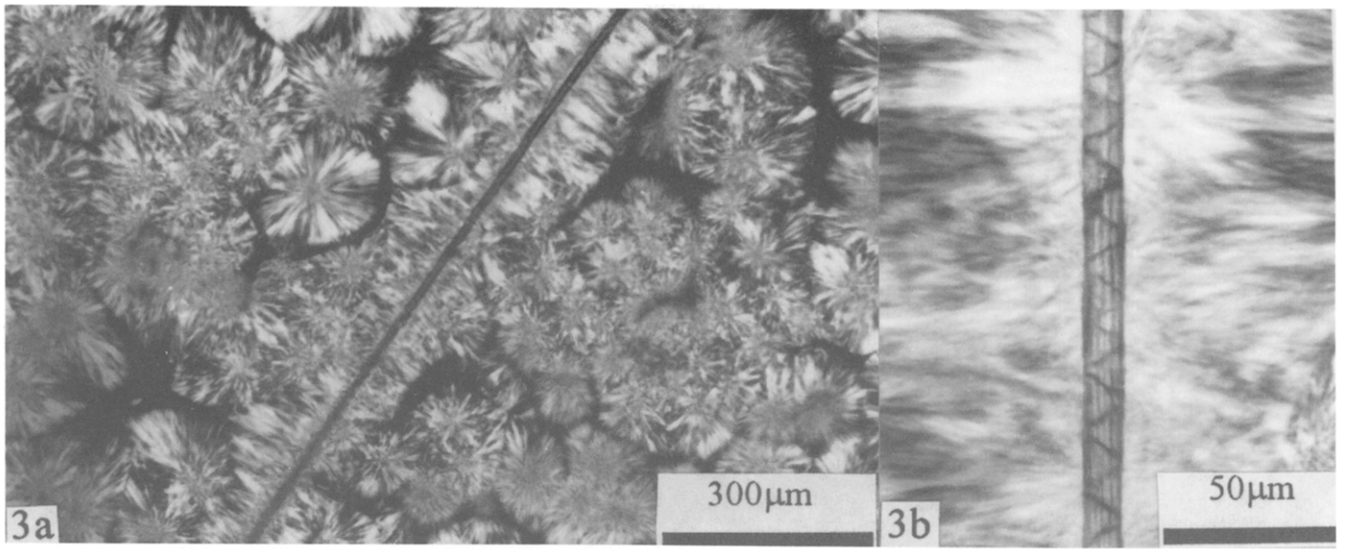

Figure 3 Optical micrographs of an SCTC sample showing (a) the thick transcrystalline layer and large matrix spherulites, the dark lines between bodies are cracks produced on cooling, and (b) continuous kind bands along the fibre (crossed polarizers)

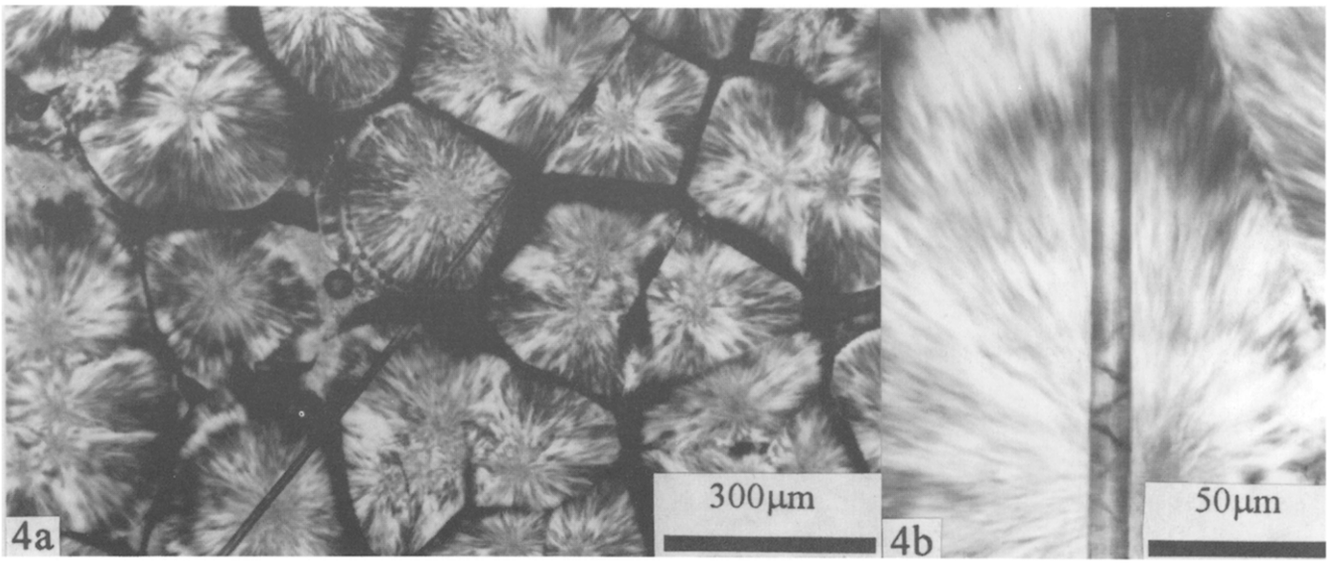

Figure 4 Optical micrographs of an SCS sample showing (a) the wholly spherulitic matrix, the dark lines between bodies are cracks produced on cooling, and (b) sporadic kink bands along the fibre (crossed polarizers)

varied with the thermal history used. SCS exhibited only a few kink bands. About half of these were associated with spherulite boundaries, often where the fibre was sheared between displaced spherulites. The FCTC and SCTC samples exhibited continuous kink bands from $+200 \pm 15\,\mu m$ and $+325 \pm 10\,\mu m$ respectively from the emergent end. It must be noted that the presence of kink bands causes the stress–strain curve, as measured by Raman spectroscopy, to be non-linear for fibres in compression. When the fibre is saturated with kink bands, any increase in the compressive strain does not result in any further change in the compressive stress[22–24].

The dark lines between major matrix features in *Figures 3a* and *4a* (SCTC and SCS) are cracks. These appeared at about 110°C during cooling from the crystallization temperature and are not present in FCTC samples. Within the matrix, spherulite boundaries and boundaries between spherulites and transcrystallinity are weaker than the microstructure within the matrix bodies. Thus, during the thermal compression during cooling, the bulk compression is hampered by a morphology composed of large microstructural units held together by relatively weak material. The problem is exacerbated by the sample's thinness ($103 \pm 3\,\mu m$) and that it rests on glass. The result is that as the matrix contracts, it is unable to accommodate bulk sample shrinkage and the weak boundary material between the units becomes stretched and may crack.

Figures 5, *6* and *7* each show the derived stress distributions along a single fibre after incrementally increasing fibre displacements for the FCTC, SCTC and

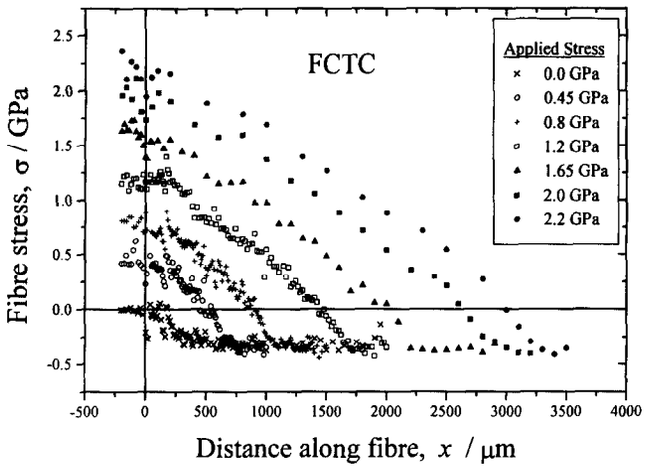

Figure 5 Pull-out data from an FCTC sample. Each point was obtained from a Raman spectrum taken at the x position on the fibre

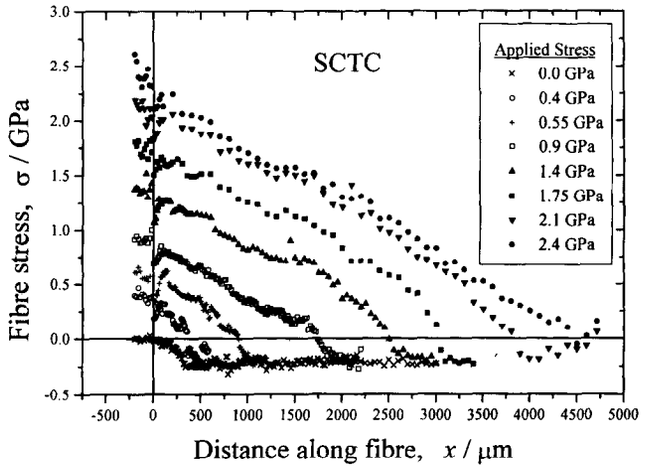

Figure 6 Pull-out data from an SCTC sample. Each point was obtained from a Raman spectrum taken at the x position on the fibre

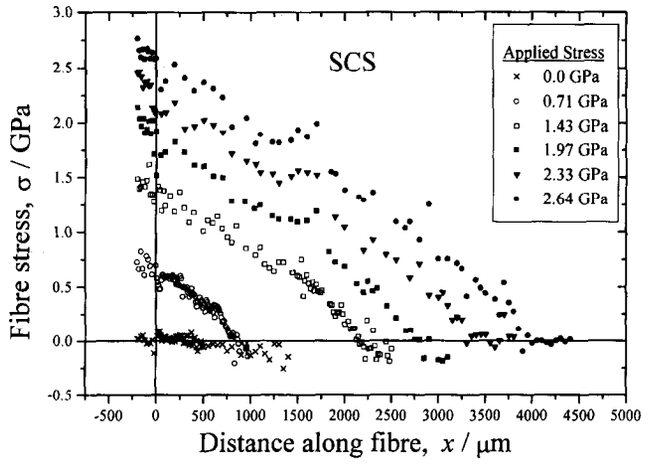

Figure 7 Pull-out data from an SCS sample. Each point was obtained from a Raman spectrum taken at the x position on the fibre

SCS samples, respectively. The point $x = 0$ is where the fibre emerges from the matrix; a negative value of x represents free fibre, and a positive value of x represents the embedded fibre.

Before pulling the fibre, the residual stress in the embedded fibre was measured. This starts at $\sigma = 0$ GPa at the embedded end, and decreases to about $\sigma = -0.3$ GPa further inside the matrix. As mentioned previously, once the formation of kink bands has saturated, the residual compressive stress in the fibre does not increase any further[22–24].

On applying stress to the fibre, measurements show that the stress on the fibre outside the matrix remained constant. Around $x = 0$ there was often a discontinuity in stress, which is associated with the complicated stresses associated with the geometry of the emergent end[25]. The fibre stress then decreased linearly with distance until it fell off in a sharp non-linear manner until gradually tailing into the residual stress region for that portion of the fibre. Some of the stress distributions can be described using two or more successive regions of linear gradient before the non-linear region, some remain linear until the stress is the same as that of the residual stress.

ANALYSIS AND DISCUSSION

The pull-out results have been modelled using a partial debonding theory[15]. This is a combination of the total bonding, elastic transfer model and the total debonding, frictional transfer model, which were proposed by Piggott[26,27]. The partial debonding theory was recently modified for the single-fibre pull-out test by Bannister *et al.*[15].

Figure 8 is a typical theoretical fibre stress distribution for partial debonding during pull-out (without residual stress). The distribution has two parts: a linear region of total debonding where the stress distribution is governed by friction, and a second part where the stress distribution is non-linear, the stress being transferred elastically into the matrix.

To apply the theory for data with compressive residual stresses, the fibre stress distribution in the

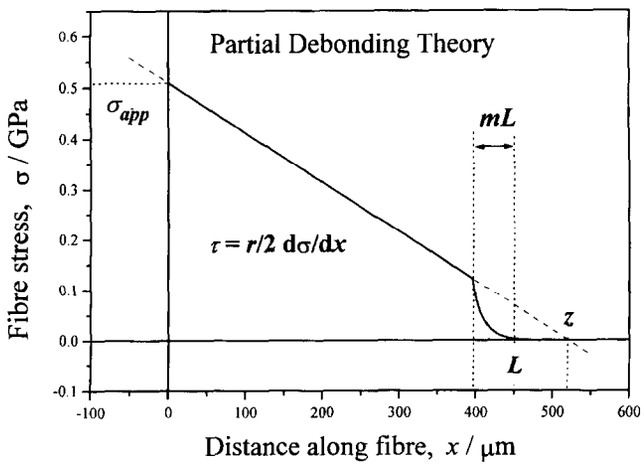

Figure 8 Theoretical plot for partial debond during pull-out showing the variation of fibre stress with distance along the fibre (without residual stress)

absence of residual stresses must first be calculated. Once these have been calculated the residual compressive stress is then subtracted from the theoretical curve to fit the original data. All terms in the following equations refer to the zero residual stress theoretical curve (*Figure 8*).

Equation (1) expresses the fibre axial stress in the linear region between $x = 0$ and $x = (1 - m)L$:

$$\sigma(x = 0, (1 - m)L) = \sigma_{app} - \frac{\sigma_{app}}{z}x \qquad (1)$$

where σ_{app} is the applied stress; $z(x)$ is a construction point marking the x-axis intercept of the linear region (were it to be extended); and m is the fraction of the distance L which is elastic. The gradient of this line is the interfacial frictional shear stress τ_i given by[15]

$$\tau_i(x = 0, (1 - m)L) = \frac{\sigma_{app}}{z} \qquad (2)$$

The elastic region of the stress distribution, from $x = (1 - m)L$ to either the end of the fibre, or where the stresses have fallen to zero (in either case this is called L), is given by[15]

$$\sigma(x - (1 - m)L, L) = \frac{2\tau_i}{r}(z - (1 - m)L)\frac{\sinh[(n(mL - x))/r]}{\sinh[nsm]} \qquad (3)$$

where

$$n^2 = \frac{E_m}{E_f}\frac{1}{\ln(R/r)}\frac{1}{(1 + \nu_m)} \qquad (4)$$

and where $s = L/r$, the fibre aspect ratio; $(1 - m)L$ is the length over which the stress distribution is linear; r is the fibre radius; E_m is the matrix tensile modulus; E_f is the fibre tensile modulus; R is the effective radius of the interface; and ν_m is the matrix Poisson's ratio.

To model stress distributions with more than one linear region, two or more z construction points are needed with suitable m fractions.

From this model, the maximum interfacial shear stress (τ_{max}) can be predicted. This is given by differentiating equation (3) and substituting into the balance of forces equation[15]. Thus the interfacial shear stress distribution in the elastic region (τ) is

$$\tau(x = (1 - m)L, L) = \frac{n\tau_i}{r}(z - (1 - m)L)\frac{\cosh[(n(mL - x))/r]}{\sinh[nsm]} \qquad (5)$$

where $\tau = \tau_{max}$ at $x = (1 - m)L$, the transition from the bonded to the debonded zone.

Figure 9 shows three fits of the experimental pull-out data to the partial debonding theory, showing a good correlation for the SCTC sample. The highest applied stress curve shown possesses two linear zones before the elastic zone is reached.

Using the partial debonding theory, three parameters have been calculated for each of the three thermal histories. These are τ_i, τ_{max} and the matrix modulus E_m, which can also be generated. The mean values for each

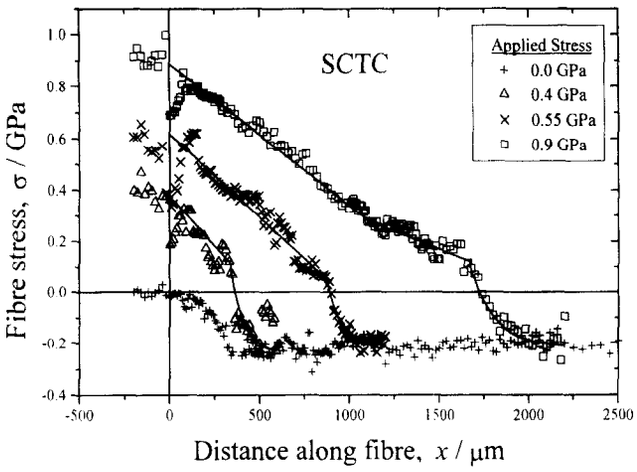

Figure 9 Theoretical modelling of the experimental SCTC pull-out data using the partial debonding model

Table 1 Comparison of parameters determined using the partial debonding theory. The number in parentheses is the number of fits from which each result was derived

	FCTC	SCTC	SCS
τ_i (MPa)	2.21 ± 0.16 (19)	2.14 ± 0.23 (19)	1.49 ± 0.13 (18)
τ_{max} (MPa)	10.6 ± 1.1 (16)	11.67 ± 1.5 (10)	8.8 ± 1.3 (10)
E_m (GPa)	0.61 ± 0.10 (16)	0.84 ± 0.19 (10)	0.77 ± 0.36 (9)

thermal history are presented in *Table 1*. Calculations used the following parameters: $E_f = 103$ GPa and fibre radius $r = 5.85\,\mu$m. The value of R was chosen so that the ratio $R/r = 4$[15], which is a typical ratio for stiff matrices. The Poisson's ratio for bulk polypropylene, $\nu_m = 0.35$, was used in the absence of values specific to transcrystalline polypropylene.

No significant differences have been found between the calculated values of τ_{max} or E_m; the average values for all samples are $\langle\tau_{max}\rangle = 10.4 \pm 2.3$ MPa and $\langle E_m\rangle = 0.74 \pm 0.42$ GPa, respectively. Any difference between the values for the different thermal histories, however, may be hidden by the errors. There is a significant difference between the τ_i for FCTC and SCS, and a probable significant difference between the τ_i for SCTC and SCS. There is no significant difference, however, between the C_i values for SCTC and FCTC.

The greater value of τ_i of the transcrystalline samples than for the spherulitic samples could be explained by the effect of the large number of kink bands present in transcrystalline samples. It has been suggested that kink bands present a rougher surface during pull-out than the original fibre surface[28], thus increasing the frictional coefficient. The SCTC and FCTC samples certainly have considerably more kink bands than SCSS samples (*Figures 2–4*), and the value of τ_i is larger.

The variation in interfacial frictional shear stress along the fibre, which resulted in a series of straight lines with different gradients, seemed to be associated with areas of the fibre on which it was difficult to focus through the surrounding matrix. Such areas were often found where the lines changed slope. For most such pairs

of lines the lower frictional shear stress was the nearer to the emergent end. This suggests that the lower frictional shear stress may have been caused by a decrease in fibre radius due to the Poisson's contraction of the fibre under the higher axial fibre stresses at the emergent end.

CONCLUSIONS

Fibre stress distributions, measured using Raman spectroscopy, from both transcrystalline and spherulitic samples can be modelled using the partial debonding theory as developed by Bannister *et al.*[15]. Using this model no significant difference has been found between either τ_{max} or E_m of transcrystalline and spherulitic specimens. It has been found that transcrystalline samples exhibit significantly higher τ_i than spherulitic samples. This has been attributed to the considerable number of kink bands found in the transcrystalline samples which would roughen the fibre surface[28]; these were not found in the spherulitic samples. The kink bands have, in turn, been attributed to the bulk compression effect that the transcrystalline layer can exert on the embedded fibre.

ACKNOWLEDGEMENTS

The authors would like to thank Dr J. L. Thomason and Dr A. J. Chervenka of Shell Research for supplying the materials studied and Dr C. Y. Yue of Nanyang University, Singapore, for helpful discussions. M.H.-B. would like to thank the European Union for financial support. R.J.Y. is grateful to the Royal Society for support in the form of the Wolfson Research Professorship in Material Science. The work is part of a large programme supported by the Engineering and Physical Sciences Research Council.

REFERENCES

1 Hull, D., 'An Introduction to Composite Materials', Cambridge Solid State Science Series, Cambridge University Press, 1988
2 Hull, D., *Compos. Sci. Technol.* 1991, **42**, 57
3 Schoolenburg, G.E. and van Rooyen, A.A., *Compos. Interfaces* 1993, **1**, 243
4 Folkes, M.J. and Hardwick, S.T., *J. Mater. Sci.* 1990, **25**, 2598
5 Thomason, J.L. and van Rooyen, A.A., *J. Mater. Sci.* 1992, **27**, 889
6 Thomason, J.L. and van Rooyen, A.A., *J. Mater. Sci.* 1992, **27**, 897
7 von Jenikel, E., Teege, E. and Hinrichs, W., *Kolloid Z.* 1952, **129**, 19
8 Sukhanova, T.E., Lednický, F., Urban, J., Baklagina, Y.G., Mikhailov, G.M. and Kudryavtsev, V.V., *J. Mater. Sci.* 1995, **30**, 2201
9 Xavier, S.F. and Sharma, Y.N., *Die Ang. Makrom. Chem.* 1984, **127**, 145
10 Moon, C.-K., *J. Appl. Polym. Sci.* 1994, **54**, 73
11 Chen, E.J.H. and Hsiao, B.S., *Polym. Eng. Sci.* 1992, **32**, 280
12 Hoecker, F. and Karger-Kocsis, J., *Polym. Bull.* 1993, **31**, 707
13 Folkes, M.J. and Wong, W.K., *Polymer* 1987, **28**, 1309
14 Andrews, M.C., Day, R.J., Hu, X. and Young, R.J., *Compos. Sci. Technol.* 1993, **48**, 255
15 Bannister, D.J., Andrews, M.C., Chervenka, A.J. and Young, R.J., *Compos. Sci. Technol.* 1995, **53**, 411
16 Heppenstall-Butler, M. and Young, R.J., *J. Mater. Sci. Lett.* 1995, **14**, 1638
17 Thomason, J.L., *Plast. Rubber Compos. Process. Applic.* 1993, **20**, 265
18 Yue, C.Y. and Cheung, W.L., *J. Mater. Sci.* 1991, **26**, 870
19 Young, R.J., Characterization of interfaces in polymers and composites using Raman spectroscopy. In 'Polymer Surfaces and Interfaces II', John Wiley & Sons, 1993
20 Yeh, W.-H., Private communication
21 Young, R.J., Lu, D., Day, R.J., Knoff, W.F. and Davis, H.A., *J. Mater. Sci.* 1992, **27**, 5431
22 Vlattas, C. and Galiotis, C., *Polymer* 1994, **35**, 2335
23 Vlattas, C. and Galiotis, C., *Polymer* 1991, **32**, 1788
24 Andrews, M.C., Lu, D. and Young, R.J., *Polymer*, submitted
25 Marotzke, C., *Compos. Interfaces* 1993, **1**, 153
26 Chua, P.S. and Piggott, M.R., *Compos. Sci. Technol.* 1985, **22**, 33
27 Piggott, M.R., 'Load Bearing Fibre Composites', Pergamon Press, Oxford, UK, 1980, pp. 83–90
28 Grubb, D.T. and Li, Z.F., *J. Mater. Sci.* 1994, **29**, 203